Contents lists available at ScienceDirect

Materials Today Physics

Universal nature of the saddle states of structural excitations in metallic glasses

J. Ding [a, ***], L. Li [b, **], N. Wang [b], L. Tian [b], M. Asta [c, d], R.O. Ritchie [c, d], T. Egami [e, f, *]

[a] Center for Alloy Innovation and Design, State Key Laboratory for Mechanical Behavior of Materials, Xi'an Jiaotong University, Xi'an, 710049, China
[b] Department of Metallurgical & Materials Engineering, University of Alabama, Tuscaloosa, AL, 35487, USA
[c] Materials Sciences Division, Lawrence Berkeley National Laboratory, Berkeley, CA, 94720, USA
[d] Department of Materials Science &Engineering, University of California, Berkeley, CA, 94720, USA
[e] Department of Materials Science & Engineering and Department of Physics and Astronomy, University of Tennessee, Knoxville, TN, 37996, USA
[f] Materials Science & Technology Division, Oak Ridge National Laboratory, Oak Ridge, TN, 37831, USA

ARTICLE INFO

ABSTRACT

A widely used schematic picture of the potential energy landscape (PEL) for liquid and glass gives an impression that the pathway of moving from a valley to another through a saddle point is predetermined. However, in reality the pathway is much more stochastic and unpredictable because thermal history is wiped out at the saddle point and the pathway down is randomly chosen. Here we explain this puzzling behavior through the study of local structural evolutions in the β relaxation process by atomistic simulations of structural excitations for metallic glasses. We find that the saddle states in the PEL show universal melt-like features in short-range order and atomic dynamics, independent of thermal history and composition. We propose that the short-lived local melting at the saddle point is responsible for wiping out the prior thermal history. This explains why the activation and relaxation stages of the β process are decoupled. The findings highlight the importance of understanding the nature of the saddle states in elucidating the system dynamics, and pose a question on the current view on the system evolution in the PEL.

1. Introduction

The structural state of glass is not unique, but critically depends on thermal history, such as the cooling rate from the melt [1,2]. As-quenched glasses can undergo structural relaxation or rejuvenation upon subsequent annealing or external energy injection [3,4]. To describe such thermally- or mechanically-induced structural evolution, the concept of the potential energy landscape (PEL) has been widely used [5–7]. The PEL is a multidimensional energy surface defined in the configurational space of N atoms. The quantities of importance are the PEL of the states rapidly cooled to zero temperature $T = 0$ (also called the inherent structures), the potential energy local minima and the nature of the saddle points (also called the transition states) that separate neighboring minima, as schematically illustrated in Fig. 1. The glass state evolves in the PEL via various barrier hopping processes. Hopping from one of the local minima to another across the sub-basins is related to "fast" β processes [8–12]; corresponding hopping across a large landscape "metabasin" is associated with slow α processes.

The PEL picture succeeds in offering a descriptive view to understand the complex dynamic behavior of glass. However, a key question of how the system chooses the migration pathways in the PEL remains incompletely understood. A simple schematic presentation of the PEL, as in Fig. 1, gives the impression that the migration pathway is almost predetermined. But the topological pathway connecting local minima and saddle points in glass could be much more complex, given the multidimensional nature of the PEL. More specifically, recent modeling investigations undertaking sampling of the pathways in the configurational space for several model glasses [13–15] all observe an important phenomenon: for the elementary hopping processes in the PEL, the initial step (from a local minimum to the saddle point) and the following step (from
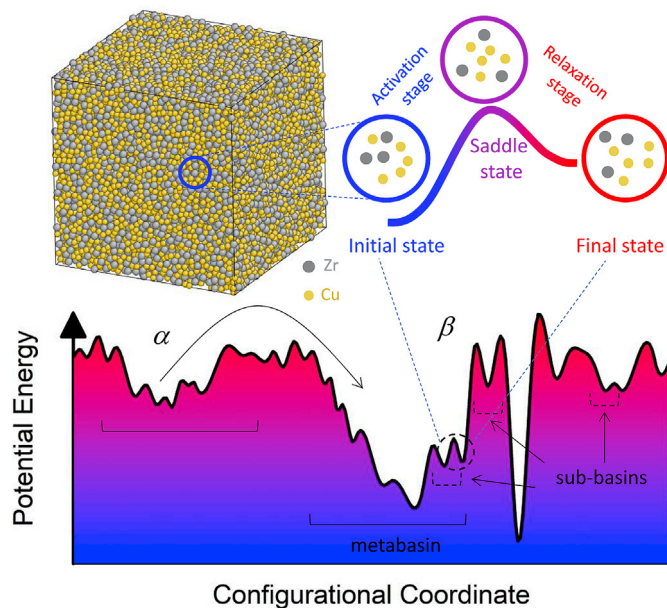
Fig. 1. Schematic description of the PEL for metallic glasses (MGs). Atomic configuration of a $Cu_{64}Zr_{36}$ MG from a molecular dynamics simulation. Schematic PEL for an MG and representative atomic reconfiguration at the initial, saddle, and final states during the elementary β process on the PEL are shown.

the saddle point to the nearby local minimum) are essentially decoupled. The glass system can lose much of its memory of prior thermal history when reaching the saddle point. Because history dependence is the hallmark of the glassy state, such memory loss at saddle states is counterintuitive. This phenomenon and many efforts on connecting PEL characteristics with glass properties, including kinetic [16], thermodynamic [15] and mechanical [17,18] behavior, require a complete understanding of the PEL. The goal of this study is to characterize the nature of the saddle states, targeting the origin of the decoupling phenomenon through the examination of atomic structural rearrangements at and near the saddle point of the PEL.

For this purpose, we focus on elementary hopping processes: namely, the hopping between neighboring local minima of the sub-basins in the PEL, also known as local structural excitations or β processes. Using atomistic simulations, we study the reconfiguration of local structure in two key stages composing the elementary process, *i.e.*, the activation stage (connecting the initial minimum and the saddle point), and the relaxation stage (connecting the saddle point to a neighboring minimum called the final state), as illustrated in Fig. 1. We discover universal short-range order (SRO) at the saddle points, independent of thermal history, and further observe a melt-like nature of the saddle points in the PEL for several model metallic glasses (MGs). We further discuss the effective temperature of saddle points, confirming its configurational molten state analogous to the liquid around the viscosity crossover temperature.

2. Results

Activation and Relaxation Energy Spectra. In this study, we investigate three model systems, $Cu_{64}Zr_{36}$, $Zr_{46}Cu_{46}Al_8$ and $Ni_{80}P_{20}$, which are representative of important MGs [19]. Moreover, $Cu_{64}Zr_{36}$ MGs were produced with five different cooling rates, spanning 10^{13} K/s to 10^9 K/s (further details are given in *Methods*). All the samples under study are designed to cover different MG systems and different cooling history in order to unravel underlying

universal properties. Each MG model contains 10,000 atoms that interact through the modified embedded-atom method potential [20,21]. The different cooling rates locate the system at different metabasins in the PEL, providing for representative sampling at different points in configurational space and allowing the effect of thermal history to be investigated. The local PEL structures are then explored by the activation-relaxation technique (ART) [13−15,22,23], an open-ended saddle point search algorithm, which is capable of providing a representative sampling of the PEL in amorphous systems (see *Methods*). Upon thermal excitation in ART, an initial perturbation is introduced by randomly displacing a small group of atoms with local connectivity to one preselected atom, called the central triggered atom. In our simulation, all the ART searches are made from the same initial configuration (*i.e.*, the same inherent structure) for each sample. All the 10,000 atoms are probed as a central triggered atom and a total of 5×10^4 searches (corresponding to 5×10^4 saddle states) are identified to produce the converged activation and relaxation energy distributions for a given MG sample.

Fig. 2A−B displays the distributions of the activation energy ΔE_{activ} (from the initial state to the saddle state), and the relaxation energy, ΔE_{relax} (from the saddle state to the final state), respectively, for the model $Cu_{64}Zr_{36}$ MGs obtained with five different cooling rates. The activation energy distributions exhibit a strong dependence on the thermal history of the samples, with the average value increasing from 1.21 eV to 1.87 eV as the cooling rate decreases from 10^{13} K/s to 10^9 K/s (Fig. 2C). Reduced cooling rates shift the ΔE_{activ} distributions to higher values, while changing their shape by reducing the (secondary) peaks around 0 eV. Similar results have been reported in Ref. [15], which also details the significance of the shape changes. Notably, the broad distribution of ΔE_{activ} manifests the diversity of atomic configurations in the amorphous structure, reflecting heterogeneous reconfigurations due to the structural excitations in the disordered MGs. In stark contrast, the distribution of the relaxation energy ΔE_{relax}, which reflects the response of the system in accommodating the atomic reconfiguration upon excitation, displays exponential decays that are insensitive to changes in cooling rate over the four orders of magnitude investigated. Consequently, the average value of ΔE_{relax} is nearly independent of the thermal history of MGs, increasing only slightly with a decrease in cooling rates (Fig. 2C). The weak correlation or decoupling between ΔE_{activ} and ΔE_{relax} indicates that the activated atoms in the saddle states largely lose the memory of their initial configurations. This same decoupling feature was also observed in earlier studies by Kallel et al. in amorphous Si [13], Swayamjyoti et al. in a binary model Lennard Jones glass [14], and Fan et al. in $Cu_{56}Zr_{44}$ MGs [15]. Accordingly, an important question to understand is what characterizes the structure of the system at the saddle state, and how it leads to the decoupling of the activation and relaxation stages of local structural excitations.

Short-Range Order (SRO) of the Initial, Saddle and Final States. To obtain a direct physical picture of local structural excitations occurring at the atomic scale, we conduct here a detailed structural analysis of the central triggered atoms in the ART process, focusing in particular on the SRO features. This focus on the central triggered atoms is motivated by the fact that thermally-activated structural excitations in MGs are highly localized, involving only a small number of atoms [14,24]. The structural metric is based on the degree of a local order [19], which is classified into three groups of SRO: icosahedral, icosahedral-like, and more distorted liquid-like atomic configurations. Specifically, the icosahedral atomic configurations are the characteristic SRO features for each MG, such as Cu-centered full icosahedra with Voronoi index <0, 0, 12, 0> for $Cu_{64}Zr_{36}$ MG, Ni-centered <0, 1, 10, 2> and P-centered <0, 2, 8, 0> for $Ni_{80}P_{20}$ MG as well as Cu-centered and Al-

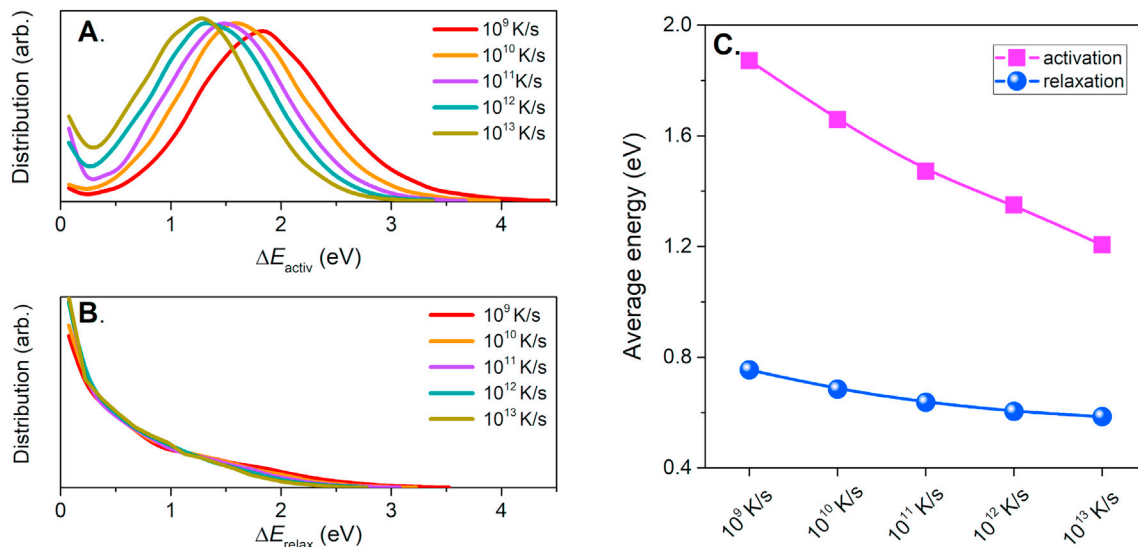**Fig. 2.** Activation and relaxation energy spectra. (A)–(B) The activation and relaxation energy spectra, respectively, of $Cu_{64}Zr_{36}$ MGs with cooling rates from 10^9 K/s to 10^{13} K/s. (C) The average value of the activation energy and relaxation energy *vs.* cooling rates from 10^9 K/s to 10^{13} K/s.

centered <0, 0, 12, 0> for $Zr_{46}Cu_{46}Al_8$ MG. Supplementary Table 1 lists the Voronoi indices of the three groups used to capture the key structural features of these glass systems [19,21,25,26].

Fig. 3 displays the fractions of the three SRO groups at the (A) initial, (B) saddle, and (C) final states, upon local structural excitation, for $Cu_{64}Zr_{36}$ MG samples across the five different cooling rates. At the initial state, shown in Fig. 3A, the cooling rates significantly influence the SRO features. The fast-quenched MG retains a large number of liquid-like atoms, whereas the slowly-cooled samples have more solid-like icosahedral atoms. This trend is expected and consistent with previous simulation results [25]. At the final states, shown in Fig. 3C, the SRO structures become more disordered for all the samples, showing a much weaker dependence on thermal history when compared with the initial states.

In contrast, at the saddle state in Fig. 3B, the statistics of the SRO of the central triggered atoms become virtually independent of cooling history. The samples with different cooling histories exhibit similar SRO statistics at the saddle state with $3.8 \pm 0.1\%$ of icosahedral atoms, $51.6 \pm 0.6\%$ of icosahedral-like atoms, and $44.6 \pm 0.6\%$ liquid-like atoms. This observation is important, considering the striking difference in the initial configurations (Fig. 3A). The most logical hypothesis to produce such invariant SRO statistics at saddle states is that the local regions resemble a *special form of melt*. In other words, when the system reaches the saddle states, the local

region configurationally melts for a short time, wiping out the processing history in that local region. Upon relaxation, the melt droplet solidifies in the glass matrix, and the memory of thermal history is partially recovered due to the constraints of the neighboring atoms. This idea of a melt-like transition to reach saddle states would naturally explain why the system loses memory of the initial configurations. It should be cautioned that the system in the excited state is in a transient state far from equilibrium, so the usual sense of the phase, such as the liquid phase, does not apply. For instance, the equipartition between the potential energy and the kinetic energy is not expected. Most likely the system would have little kinetic energy and most of the energy resides in the potential energy. Therefore, we call this melt-like region as a "configurationally molten" state. Further characteristics of this configurationally molten state are described below.

Nature of the Configurationally Molten State. As discussed in the previous section, we hypothesize that the activated local regions at the saddle states are in a configurationally molten state. We further characterize this state by finding the equivalent transient state of a sample with the same SRO statistics as that of activated local regions (Fig. 3). This is achieved by instantly reducing the temperature of the equilibrium liquid phase to an extremely low temperature (*e.g.*, $T_{relax} = 10$ K), followed by structural relaxation at T_{relax} to reach the inherent structure. This
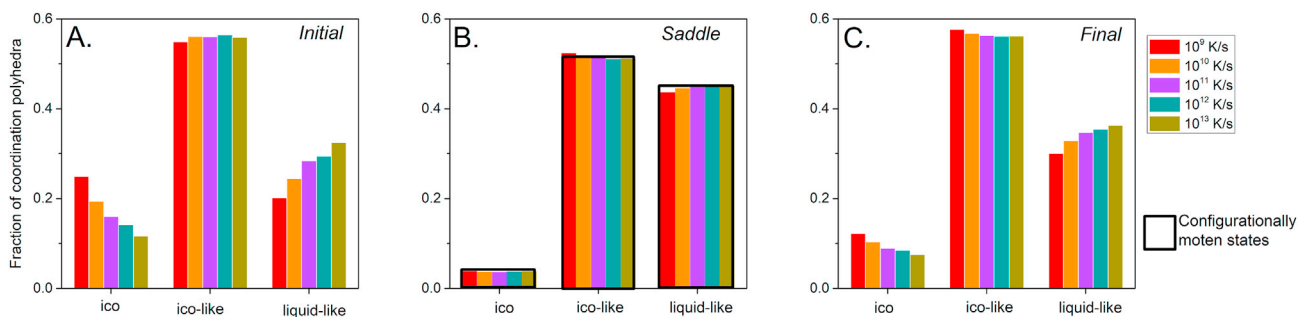

Fig. 3. SRO analysis of activation and relaxation stages. (A–C) The distribution of three groups of characteristic coordination polyhedra, including icosahedral, icosahedral-like, and liquid-like types, around the central triggered atoms within $Cu_{64}Zr_{36}$ MG configurations quenched from various cooling rates, at the initial, saddle and final state, respectively, upon thermal excitation.

method is designed to minimize structural relaxation by eliminating thermal vibration. Fig. 4A illustrates an example for the $Cu_{64}Zr_{36}$ model MG, illustrating how the potential energy of a melt (initially at T_{ini} = 2000 K) relaxes with time at T_{relax} = 10 K, approaching its inherent structure. At the same time, the SRO of the transient state during relaxation is compared to that of the saddle state probed by elementary hopping (or β process). The corresponding total deviation of the SRO, Δf_{sum}, was monitored by computing the sum of the changes in the fractions of icosahedral, icosahedral-like and liquid-like coordination polyhedra (as used in Fig. 3A–C and defined in Supplementary Table 1):

$$\Delta f_{sum} = |f_{ico} - f_{ico,saddle}| + |f_{ico-like} - f_{ico-like,saddle}| + |f_{liquid-like}$$
$$- f_{liquid-like,saddle}|$$

$$(1)$$

where $f_{ico,\ saddle}$, $f_{ico-like,\ saddle}$ and $f_{liquid-like,\ saddle}$ are the fraction of three groups of characteristic SRO at the saddle state (e.g., shown in Fig. 3B) of MGs upon thermal excitation; f_{ico}, $f_{ico-like}$ and $f_{liquid-like}$ are the corresponding SRO fractions during structural relaxation at T_{relax}, as described above.

Interestingly, Δf_{sum} reaches a minimum (of almost zero) after 2 ps in Fig. 4A, which coincides with the crossover of potential energy change during relaxation, as denoted in this figure. We thereby identify the system at this instance as the "configurationally molten state", where the corresponding f_{ico}, $f_{ico-like}$, and $f_{liquid-like}$ of $Cu_{64}Zr_{36}$ are also plotted in Fig. 3B, confirming that the configurationally molten state has almost the same SRO statistics as the central triggered atoms at the saddle state in the glassy samples. The structural resemblance is reproducible for the configurationally molten state obtained from different initial and relaxation configurations (i.e. T_{ini} and T_{relax}, see Supplementary Fig. 2).

In addition to $Cu_{64}Zr_{36}$, another two MG systems, specifically $Zr_{46}Cu_{46}Al_8$ and $Ni_{80}P_{20}$, have also been analyzed to demonstrate the universal nature of the configurationally molten state. $Zr_{46}Cu_{46}Al_8$ is a ternary MG with characteristic icosahedral SRO of Cu- and Al-centered <0, 0, 12, 0>, while the metal-metalloid $Ni_{80}P_{20}$ MG contains Ni-centered <0, 1, 10, 0> and P-centered <0, 2, 8, 0> clusters characterizing the icosahedral SRO. As shown in Fig. 4B, similar to $Cu_{64}Zr_{36}$ MGs (with five different cooling rates), the three SRO polyhedral fractions (icosahedral, icosahedral-like, and liquid-like) of $Zr_{46}Cu_{46}Al_8$ MG and $Ni_{80}P_{20}$ MG also exhibit a

good consistency of SRO features between the saddle state in glassy samples and the corresponding configurationally molten state.

Furthermore, we look into the potential energy of the configurationally molten state. For $Cu_{64}Zr_{36}$ MGs, its configurationally molten state (obtained with T_{ini} = 2000 K and T_{relax} = 10 K) has a potential energy higher than that of the slowest-cooled (10^9 K/s) MG by ΔE_p = 76 meV. According to the equipartition theorem in the liquid state [27], this could translate to $\Delta E_p = (3/2)k\Delta T$, with ΔT = 588 K. Considering T_g = 760 K for this slowest-cooled $Cu_{64}Zr_{36}$ MG, the effective temperature of the configurationally molten state is $T_{eff} = T_g + \Delta T$ = 1348 K, after 2 ps relaxation. This temperature is close to its liquidus temperature (T_l ~1250 K [28]) and just below the viscosity crossover temperature (T_A ~ 1600 K for $Cu_{56}Zr_{44}$ [29]). Therefore, the configurationally molten state could correspond to a liquid with low viscosity, and melts in about 1–2 ps (Fig. 4A), effectively eliminating the thermal history of the inherent glass structure. This finding provides strong evidence for the similarity between the thermally-excited saddle state for glassy samples and the configurationally molten state with an effective temperature close to its liquidus temperature T_l. To the best of our knowledge, this is the first time the nature of the MG at the saddle states has been revealed to be a molten liquid. The localized configurationally molten state at the saddle states sheds light on the physics of elementary processes in the PEL.

Evolution of Atomic Structure by Thermal Excitation. The evolution of the atomic structure around the central triggered atoms in real space is characterized to assess the spatial extent of the regions affected by the excitation. Fig. 5A–B displays the fractions of icosahedral atoms in the first few shells around the central triggered atoms at the saddle and final states, respectively for $Cu_{64}Zr_{36}$ MGs. At the saddle states, as before (Fig. 3B), the fraction of the icosahedral clusters of the central atoms collapses to a value of ~ 4%. Moving outward from the central triggered atoms, the icosahedral fraction increases rapidly, and in the third nearest shells they completely revert to the atomic configurations corresponding to the initial states. Such observations are consistent with the spatial variation of elevated atomic potential energy as shown in Supplementary Fig. 1, as well as the estimate in ref. [30]. An important finding is that the size of the excited zone is about two neighboring shells, regardless of the initial states. This observation confirms the local nature of the structural excitation in the MG [14,22]. Moreover, the atomic rearrangements which trigger such
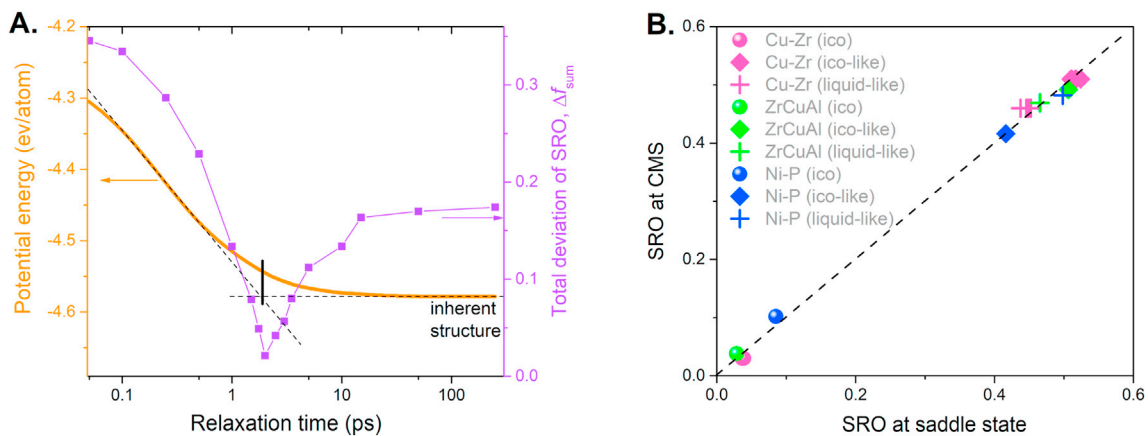

Fig. 4. SRO of the configurationally molten state (A) Preparation of the configurationally molten state by instantly reducing the temperature of melts from T_{ini} = 2000 K to T_{relax} = 10 K, followed by structural relaxation at T_{relax}. The corresponding potential energy and Δf_{sum}, are shown with relaxation time. (B) The three SRO polyhedral fractions (icosahedral, icosahedral-like, and liquid-like) for $Cu_{64}Zr_{36}$, $Zr_{46}Cu_{46}Al_8$ and $Ni_{80}P_{20}$ MG are plotted between the saddle state in glassy samples and the corresponding configurationally molten state (CMS).
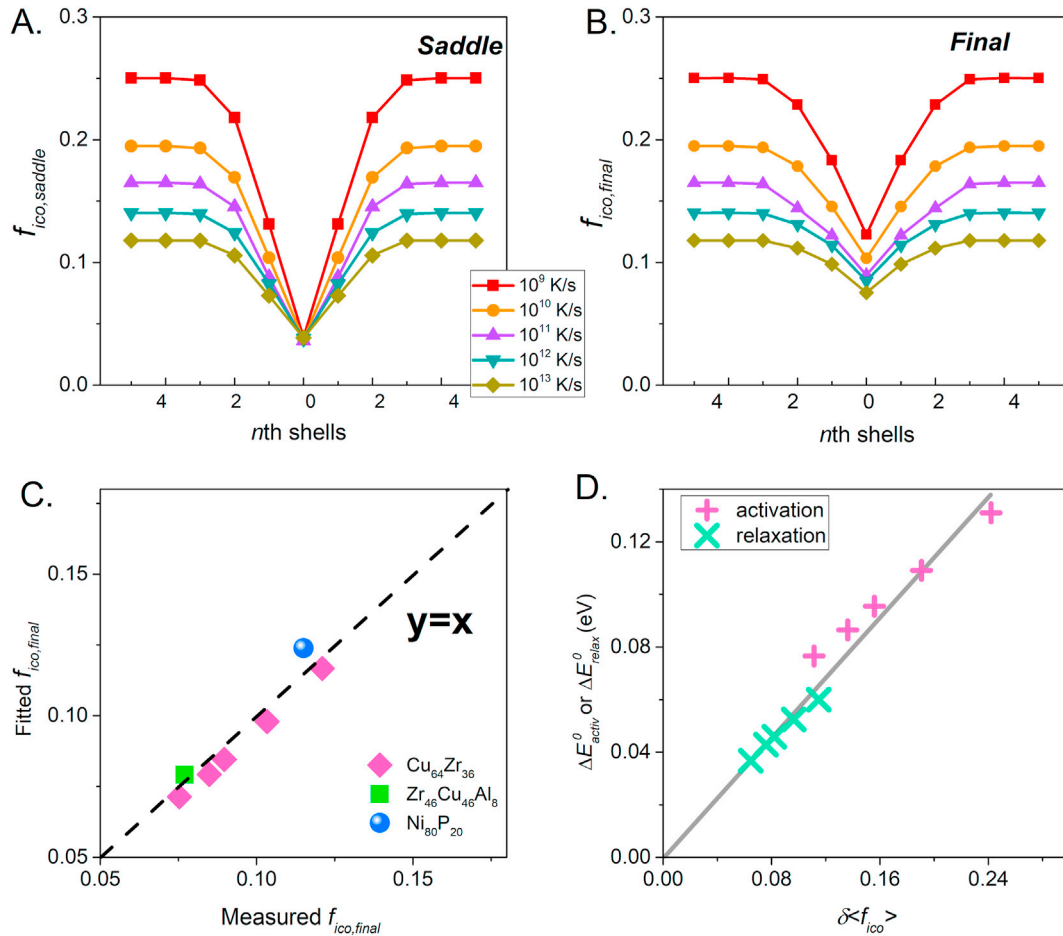
Fig. 5. Evolution of SRO during activation and relaxation (A–B) For the $Cu_{64}Zr_{36}$ MGs, the fraction of icosahedral clusters *vs.* the number of shells departed away from the central triggered atoms at the saddle and final state, respectively, for all cooling rates. (C) The fitted *vs.* the measured icosahedral fraction of the central triggered atoms at the final states for the $Cu_{64}Zr_{36}$ MGs (with five different cooling rates), $Zr_{46}Cu_{46}Al_8$ and $Ni_{80}P_{20}$ MGs. (D) The difference in the activation/relaxation energy per atom *vs.* the difference of the fraction of the icosahedral atom between the initial/final and saddle state $\delta\langle f_{ico}\rangle$, respectively for $Cu_{64}Zr_{36}$ MGs with five different cooling rates.

elementary excitations are independent of the cooling history, which is consistent with the previous work of Fan et al. [15].

In the relaxation stage, the neighboring atoms play some role in accommodating the triggered atoms. From Fig. 5 at the final states, the central triggered atoms and their closest neighbors relax towards, but do not go back to, the corresponding initial states, which gives rise to the weak dependence of ΔE_{relax} on cooling rate (Fig. 2C). In fact, the configurations of the central triggered atoms at the final states resemble, to a higher degree, their SRO at the saddle state. We propose a simple equation to fit the icosahedral fractions of the central triggered atoms at the final states, $f_{ico,final}$, with respect to the values at initial $f_{ico,initial}$ and saddle states $f_{ico,saddle}$ shown in Fig. 5C. A linear relationship $f_{ico,final} = 0.75 \times f_{ico,saddle} + 0.36 \times f_{ico,initial}$ emerges between the fitted and measured values for the $Cu_{64}Zr_{36}$ MGs (with five different cooling rates), $Zr_{46}Cu_{46}Al_8$ and $Ni_{80}P_{20}$ MGs, in which the contribution of the saddle states in determining the SRO at the final states is about twice that at the initial states, demonstrating quantitatively the significance of the saddle states.

Moreover, the relationships between the potential energy change and the change in the icosahedral fraction of the central triggered atoms for both the activation and relaxation stages are shown in Fig. 5D for $Cu_{64}Zr_{36}$ MGs with five different cooling rates. Using the saddle state as a reference configuration, both the activation and relaxation energies linearly scale with the changes in the

fraction of icosahedral clusters $\delta\langle f_{ico}\rangle$ for all the five cooling samples, where:

$$\delta\langle f_{ico}\rangle = \sqrt{\left(f_{ico,final}\right)^2 - \left(f_{ico,saddle}\right)^2} \; or \; \sqrt{\left(f_{ico,initial}\right)^2 - \left(f_{ico,saddle}\right)^2}$$

(2)

This simple relationship implies that the descent paths from the saddle states towards the surrounding local minima can be interpreted as a sequence of independent random steps, regardless of what the initial states or final states are, adding evidence for the configurationally molten nature of the saddle points.

Atomic Dynamics of the Saddle States upon Thermal Excitation. The atomic dynamics associated with crossing the saddle state in structural excitations in MGs are also non-trivial, with the cage-breaking atomic jump found to be strongly related with the β relaxation [31]. Here we compare the atomic dynamics across the saddle state of the β relaxation with the elementary excitations in the liquid state. Fig. 6 exhibits the average number of lost/gained nearest neighbors around central triggered atoms into the final states within $Cu_{64}Zr_{36}$ MG configurations quenched from five cooling rates as well as the $Ni_{80}P_{20}$ and $Zr_{46}Cu_{46}Al_8$ MGs. Interestingly, the average number of lost/gained nearest neighbors around the central triggered atoms during relaxation of the saddle state (transition from the saddle to final states) is very close to unity
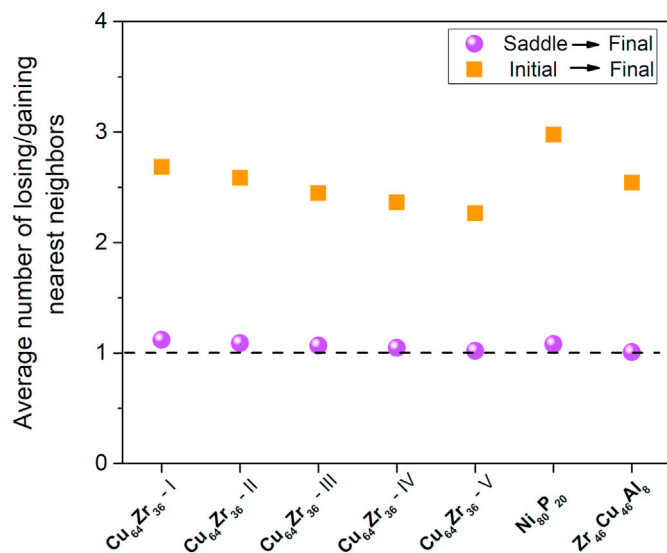
Fig. 6. Atomic dynamics features upon thermal excitation. Average number of losing/gaining nearest neighbors around the central triggered atoms of $Cu_{64}Zr_{36}$ MGs (I–V corresponding to the quenching rates of 10^9 K/s $- 10^{13}$ K/s), $Ni_{80}P_{20}$ and $Zr_{46}Cu_{46}Al_8$ MGs, from initial or saddle state to final state, upon thermal excitation.

and almost independent of the MG systems and cooling history. In contrast, the transition from the initial to final states yields more than two lost/gained nearest neighbors with noticeable dependence on MG system and cooling history. Given the previous study [29], the relaxation of the saddle state in MGs, which involves one nearest neighbor atom on average, can correspond to the local configurational excitations in the atomic connectivity network of metallic liquids at high temperatures. More specifically, the local configurational excitations were defined as having lost/gained one nearest neighbor around an atom, acting as the elementary steps to change the atomic connectivity network. These steps directly control the macroscopic viscosity, demonstrated to be the elementary excitations in metallic liquids above the viscosity crossover temperature in liquids, T_A, whereas below T_A increasing number of atoms are involved in the local excitation process [29]. Therefore, the atomic dynamics in Fig. 6 clearly demonstrate the similarity between the relaxation of the saddle states and local configurational excitation of melts, compared to the excitation from the glassy initial states; this adds additional support to the idea that the local state at the saddle point is very similar to that of a melt.

3. Discussions and conclusions

We have employed atomistic simulations to probe the saddle states of the elementary β process among different MG models ($Cu_{64}Zr_{36}$, $Ni_{80}P_{20}$ and $Zr_{46}Cu_{46}Al_8$ MGs) and different cooling history (10^{13} K/s $- 10^9$ K/s for $Cu_{64}Zr_{36}$ MGs), and observed the universal nature of the saddle points among all the MGs studied. More specifically, by probing the reconfiguration of the short-range clusters at key states on the potential energy landscape (PEL), a melt-like SRO feature is found for the central triggered atoms at the saddle states, which is independent of MG composition and thermal history. The universal melt-like nature at the saddle points is further supported by the atomic structural evolution and atomic dynamics crossing the saddle points.

From the perspective of the PEL, the local atomic rearrangements appear as saddle-point activation in the evolving system. For instance, in the glass state, it is pictured that through a sequence of the β processes (*i.e.*, hopping across "sub-basins"), the system can

move into a deeper valley in PEL (see Supplementary Fig. 3) or climb to higher-energy inherent states and eventually escape to an adjacent metabasin, leading to the emergence of the α process [6,7]. While the detailed physical nature of the pathway involved depends on the specific phenomenon (*e.g.*, on thermal excitation *vs.* mechanical deformation), an improved framework of the topologically complex PEL surface is needed to elucidate multi-level energy basins and associated nesting of saddle points. While several studies have been performed to unveil the hierarchy and roughness of the sub-basins of glasses [18,24,32], our work focuses on the underlying nature of the saddle states, identifying a universal configurational state on the transition pathway that dictates the hopping between the "sub-basins" in the PEL. Specifically, for the elementary β processes, the activation stage upon the thermal excitations pushes the local regions into a short-lived molten state, *i.e.*, to a special form of the melt, referred to as the configurationally molten state, with the effective temperature hundreds of degrees above T_g (close to liquidus temperature T_l and viscosity crossover temperature T_A). For MGs with different cooling history, the transition to the saddle states brings them always to the same effective temperature, resulting in similar SRO in spite of differing prior thermal history; this consequently removes any configurational memory of prior thermal history. It is noteworthy that this memory loss at saddle states of the isolated β processes is limited to a very small region of melting, unlike the memory loss associated with the α process (or collective behavior of β processes) which is more extended in space. In the PEL theory, however, if even a small portion of the system is in a different state, the entire system is defined to be in a different state. In the simple PEL picture in which only the inherent states are considered, the evolution of the system from one basin to the other may appear predetermined. However, in reality, the kinetic momenta of atoms, which are random in direction and magnitude, impose a large uncertainty in the process of choosing the direction away from the saddle point, making the process strongly stochastic. In fact, the nature of the saddle point as a generator of chaos even in simple systems has been known for some time [33,34]. In a complex many-body system such as glass, this chaotic nature could be even more pronounced and multi-dimensional. In our view, characterization of the system at the saddle point as "molten" aptly emphasizes the chaotic and unpredictable nature of the system in this condition.

The nature of the saddle points provides insights into the decoupling of the activation and relaxation stages of the β process observed in several disordered systems [13–15]. It is also consistent with the results of an early measurement of internal friction, which suggested the universality of the saddle point energy [35]. Furthermore, it could help to explain why the shear-transformation-zone (STZ) is an emergent quantity, which does not pre-exist before action and disappears afterward in the STZ theory [36–40], and how the final effective temperature of STZ is independent of the real temperature below the glass-transition temperature [41]. Our discovery enabled by the robust sampling and dedicated analysis of the MG transient states provides an improved understanding of the PEL, and the universal feature of the saddle points should advance efforts to further explore the glass structural evolution in the PEL and to guide the search of extended glass states for practical applications.

4. Materials and methods

MG Sample Preparation. Molecular dynamics (MD) simulations were employed to prepare and analyze three model metallic glasses: $Cu_{64}Zr_{36}$, $Zr_{46}Cu_{46}Al_8$ and $Ni_{80}P_{20}$. These simulations made use of optimized embedded-atom-method (EAM) potentials and the open-source LAMMPS software [42]. Samples containing

10,000 atoms were equilibrated in the high-temperature liquid state at 2500 K for 10 ns and then quenched to 0 K at fixed volume using an NVT ensemble (*e.g.,* the sample sizes of $Cu_{64}Zr_{36}$ MGs were fixed at 54.27 Å × 54.27 Å × 54.27 Å). Five different cooling rates, spanning 10^{13} K/s to 10^9 K/s, were applied for $Cu_{64}Zr_{36}$ MGs, while the other two MGs, $Zr_{46}Cu_{46}Al_8$, and $Ni_{80}P_{20}$ MGs, were quenched with the cooling rate of 10^{10} K/s. Periodic boundary conditions (PBC) were applied in all three directions during MD simulations [43]. Voronoi tessellation analysis was employed to investigate the coordination polyhedra based on nearest neighbor atoms determined for the inherent structure of the MGs [19].

Activation-Relaxation Technique (ART). Upon structural excitation in ART, an initial perturbation is introduced by randomly displacing a small group of atoms with local connectivity to a central triggered atom. The magnitude of initial random perturbation is small with a fixed step size of ~ 0.1 Å. Following the random displacement step, 5 relaxation steps are imposed perpendicularly to the direction of motion, allowing the total energy and forces of the system under control. Several iterations of such steps are applied until a negative eigenvalue of the Hessian appears to push the initial equilibrium configuration out of its basin. Using the local Hessian structure of the PEL, the searching algorithm in ART allows the system to climb out of its initial energy sub-basin, converge to a connected saddle state, and eventually relax to a nearby sub-basin [13–15,22,23,44]. In our simulations, all the ART searches were from the same initial configuration (*i.e.,* the same inherent structure) for each sample. All the 10,000 atoms were probed as a central triggered atom for at least 20 successful ART searches with different perturbation directions. Consequently, more than 2×10^5 ART searches were collected in total. After removing the redundant searches, ~ 5×10^4 structural rearrangements were identified to produce the converged activation and relaxation energy spectra for a given MG sample.

Credit author statement

Conceptualization was made by JD, LL, MA, ROR and TE. Methodology was chosen by JD, LL, MA, and TE. Investigation was made by JD, LL, NW and LT. Writing carried out by JD, LL, MA, ROR and TE. Supervision made by JD, LL, MA, ROR and TE.

Data availability

Data can be made available on request to the corresponding authors.

Declaration of competing interest

The authors declare that they have no known competing financial interests or personal relationships that could have appeared to influence the work reported in this paper.

Acknowledgments

Appendix A. Supplementary data

Supplementary data to this article can be found online at https://doi.org/mmcdoino.

References

[1] E. Donth, The Glass Transition: Relaxation Dynamics of Liquids and Disordered Materials, Springer, Berlin, 2010.
[2] A.L. Greer, Metallic glasses, in: D.E. Laughlin, K. Hono (Eds.), Physical Metallurgy, Elsevier, 2014, pp. 305–385.
[3] S.V. Ketov, et al., Rejuvenation of metallic glasses by non-affine thermal strain, Nature 524 (2015) 200–203.
[4] A. Das, P.M. Derlet, C. Liu, E.M. Dufresne, R. Maas, Stress breaks universal aging behavior in a metallic glass, Nat. Commun. 10 (2019) 5006.
[5] M. Goldstein, Viscous liquids and the glass transition: a potential energy barrier picture, J. Chem. Phys. 51 (1969) 3728.
[6] P.G. Debenedetti, F.H. Stillinger, Supercooled liquids and the glass transition, Nature 410 (2001) 259.
[7] D.J. Wales, A microscopic basis for the global appearance of energy landscapes, Science 293 (2001) 2067.
[8] H.B. Yu, W.H. Wang, K. Samwer, The β relaxation in metallic glasses: an overview, Mater, Today Off. 16 (2013) 183.
[9] H.B. Yu, W.H. Wang, H.Y. Bai, K. Samwer, The β-relaxation in metallic glasses, National Sci. Rev. 1 (2014) 429.
[10] G.P. Johari, M. Goldstein, Viscous liquids and the glass transition. II. Secondary relaxations in glasses of rigid molecules, J. Chem. Phys. 53 (1970) 2372.
[11] H.B. Yu, R. Richert, K. Samwer, Structural rearrangements governing Johari-Goldstein relaxations in metallic glasses, Sci. Adv. 3 (2017) 1701577.
[12] F. Zhu, et al., Intrinsic correlation between β-relaxation and spatial heterogeneity in a metallic glass, Nat. Commun. 7 (2016) 11516.
[13] H. Kallel, N. Mousseau, F. Schiettekatte, Evolution of the potential-energy surface of amorphous silicon, Phys. Rev. Lett. 105 (2010): 045503.
[14] S. Swayamjyoti, J.F. Löffler, P.M. Derlet, Local structural excitations in model glasses, Phys. Rev. B 89 (2014) 224201.
[15] Y. Fan, T. Iwashita, T. Egami, Energy landscape-driven non-equilibrium evolution of inherent structure in disordered material, Nat. Commun. 8 (2017) 15417.
[16] W.L. Johnson, M.D. Demetriou, J.S. Harmon, M.L. Lind, K. Samwer, Rheology and ultrasonic properties of metallic glass-forming liquids: a potential energy landscape perspective, MRS Bull. 32 (2007) 644–650.
[17] W.L. Johnson, K. Samwer, A universal criterion for plastic yielding of metallic glasses with a $(T/Tg)^{2/3}$ temperature dependence, Phys. Rev. Lett. 95 (2005) 195501.
[18] P.H. Cao, M.P. Short, S. Yip, Potential energy landscape activations governing plastic flows in glass rheology, Proc. Natl. Acad. Sci. Unit. States Am. 116 (2019) 18790–18797.
[19] Y.Q. Cheng, E. Ma, Atomic-level structure and structure-property relationship in metallic glasses, Prog. Mater. Sci. 56 (2011) 379–473.
[20] Y.Q. Cheng, E. Ma, H.W. Sheng, Atomic level structure in multicomponent bulk metallic glass, Phys. Rev. Lett. 102 (2009) 245501.
[21] H.W. Sheng, E. Ma, M.J. Kramer, Relating dynamic properties to atomic structure in metallic glasses, JOM 64 (7) (2012) 856–881.
[22] G.T. Barkema, N. Mousseau, Event-based relaxation of continuous disordered systems, Phys. Rev. Lett. 77 (1996) 4358.
[23] D. Rodney, C.A. Schuh, Distribution of thermally activated plastic events in a flowing glass, Phys. Rev. Lett. 102 (2009) 235503.
[24] Y. Fan, T. Iwashita, T. Egami, How thermally activated deformation starts in metallic glass, Nat. Commun. 5 (2014) 5083.
[25] J. Ding, Y.Q. Cheng, E. Ma, Full icosahedra dominate local order in $Cu_{64}Zr_{34}$ metallic glass and supercooled liquid, Acta Mater. 69 (2014) 343–354.
[26] J. Ding, et al., Universal structural parameter to quantitatively predict metallic glass properties, Nat. Commun. 7 (2016) 13733.
[27] V.A. Levashov, R.S. Aga, J.R. Morris, T. Egami, Equipartition theorem and the dynamics of liquids, Phys. Rev. B 78 (2008): 064205.
[28] D. Arias, J.P. Abriata, Cu-Zr (Copper-Zirconium), Bull. Alloy. Phase. Diagram. 11 (1990) 5.
[29] T. Iwashita, D.M. Nicholson, T. Egami, Elementary excitations and crossover phenomenon in liquids, Phys. Rev. Lett. 110 (2013) 205504.
[30] Y. Fan, T. Iwashita, T. Egami, Crossover from localized to cascade relaxations in metallic glasses, Phys. Rev. Lett. 115 (2015): 045501.
[31] H.B. Yu, et al., Fundamental link between β relaxation, excess wings and cage-breaking in metallic glasses, J. Phys. Chem. Lett. 9 (2018) 5877–5883.
[32] P. Charbonneau, J. Kurchan, G. Parisi, P. Urbani, F. Zamponi, Fractal free energy landscapes in structural glasses, Nat. Commun. 5 (2014) 3725.
[33] J.F. Mason, P.T. Piiroinen, Saddle-point solutions and grazing bifurcations in an

impacting system, Chaos 22 (2012): 013106.

[34] H. Párraga, F.J. Arranz, R.M. Benito, F. Borondo, Above saddle-point regions of order in a sea of chaos in the vibrational dynamics of KCl, J. Phys. Chem. 122 (2018) 3433.

[35] N. Morito, T. Egami, Internal friction and reversible structural relaxation in metallic glass $Fe_{32}Ni_{36}Cr_{14}P_{12}B_6$, Acta Metall. 32 (1984) 603.

[36] A.S. Argon, Plastic deformation in metallic glasses, Acta Metall. 27 (1979) 47.

[37] M.L. Falk, J.S. Langer, Dynamics of viscoplastic deformation in amorphous solids, Phys. Rev. E 57 (1998) 7192.

[38] M. Tsamados, A. Tanguy, C. Goldenberg, J.L. Barrat, Local elasticity map and plasticity in a model Lennard-Jones glass, Phys. Rev. E 80 (2009): 026112.

[39] N. Wang, J. Ding, F. Yan, M. Asta, R.O. Ritchie, L. Li, Spatial correlation of elastic heterogeneity tunes the deformation behavior of metallic glasses, npj Comput. Mater. 4 (2018) 19.

[40] T.C. Hufnagel, C.A. Schuh, M.L. Falk, Deformation of metallic glasses: recent developments in theory, simulations, and experiments, Acta Mater. 109 (2016) 375−393.

[41] T.K. Haxton, A.J. Liu, Activated dynamics and effective temperature in a steady state sheared glass, Phys. Rev. Lett. 99 (2007) 195701.

[42] S. Plimpton, Fast parallel algorithms for short-range molecular dynamics, J. Comput. Phys. 117 (1995) 1.

[43] M.P. Allen, D.J. Tildesley, Computer Simulation of Liquids, Clarendon Press, Oxford, 1987.

[44] L. Tian, L. Li, J. Ding, N. Mousseau, ART_data_analyzer: automating parallelized computations to study the evolution of materials, Software 9 (2019) 238−243.